Catena 113 (2014) 306–313

Contents lists available at ScienceDirect

Catena

journal homepage: www.elsevier.com/locate/catena

A new approach for regional scale interrill and rill erosion intensity mapping using brightness index assessments from medium resolution satellite images

Hossein Saadat [a], Jan Adamowski [b,*], Vahid Tayefi [c], Mohammad Namdar [d], Forood Sharifi [e], Sasan Ale-Ebrahim [d]

[a] McGill University, Macdonald Campus 21, 111 Lakeshore Road, Ste-Anne-de-Bellevue, Quebec, H9X 3V9, Canada
[b] Department of Bioresource Engineering, McGill University, Macdonald Campus 21, 111 Lakeshore Road, Ste-Anne-de-Bellevue, Quebec, H9X 3V9, Canada
[c] School of Geography, Tarbiyat Modares University, P.O. Box 13445, Tehran, Iran
[d] Forest, Range and Watershed Management Organization, Lashgark Road, Tehran, Iran
[e] Soil Conservation and Watershed Management Research Institute, P.O. Box 13445, Tehran, Iran

ARTICLE INFO

Article history:
Received 21 January 2013
Received in revised form 20 June 2013
Accepted 13 August 2013

Keywords:
Interrill and rill erosion intensity
Brightness index
Landsat ETM+ imagery
Geographic information system (GIS)
Golestan dam watershed
Ancillary layers

ABSTRACT

Having accurate soil erosion intensity/type maps using satellite imagery is not generally a difficult task. However, there are still difficulties for the generation of small scale erosion features at regional and national levels. It is even more problematic when high-resolution satellite images cannot be used due to their high cost at a regional level. The principal objective of this study is to investigate the applicability of brightness value to generate accurate interrill and rill erosion intensity maps using medium resolution satellite images at a regional level. In this study, Landsat ETM+ images are used and the Golestan dam watershed with an area of 4511.8 km^2 located at northeast of Iran is selected as the study area. In order to generate a Homogeneous Land Unit (HLU) map, three ancillary layers including slope, landform, land use and land cover, are overlayed on each other. The HLUs are used in a supportive role for identifying appropriate sampling points across the entire study area, at which the degrees of interrill and rill erosions are measured. The ground-truth erosion information collected at the 1328 locations is divided into training and reference data sets. Using the Tasseled Cap transformation technique, the brightness value of each pixel at the beginning (May), middle (July) and end (September) of growing season is obtained. By subtracting the May brightness value (B_M) from the July one (B_J), and the July brightness value from the September one (B_S), two new brightness images representing the brightness variations over May–July (B_{MJ}) and July–September (B_{JS}) are created. The two new brightness images are combined to generate a map where its pixels indicate the state (i.e. increase, I, decrease, D, and constant, C) of brightness variation over the two growing seasons. Using the measured interrill and rill erosion information at the training sampling locations, a unique relationship is found between the trend of brightness variation and the erosion intensity. This relationship is validated using the reference data sets. The results show that the proposed method is able to produce an interrill–rill erosion intensity map with an overall field-checked accuracy of 96% at this study location. The main advantages of this method are its high accuracy, its lower demands on time and funds for field work, and the ready availability of required data.

1. Introduction

Long recognized as a serious worldwide land degradation problem, soil erosion has a strong negative impact on the environment by reducing soil productivity and increasing sediment and other pollution loads into receiving water bodies (Morgan, 2005). The importance of soil erosion type/intensity maps in natural resources, agricultural, soil conservation, land management and water resources management planning and development has been recognized for decades. Over the past decades, many models have been introduced and used for creating soil erosion maps (Flanagan et al., 2001; Parsons and Wainwright, 2006; Renard et al., 1997). New technologies (e.g. satellite data) and increased computing power have led to the development of new models in the context of soil erosion mapping (Morgan, 2005). Remote sensing provides detailed information over large regions with a regular revisit capability, and can greatly contribute to regional erosion assessment (Siakeu and Oguchi, 2000; Vrieling et al., 2008). Satellite imagery can assist soil erosion assessment/mapping through (i) automatic identification of large scale erosion (Vrieling et al., 2007) and its consequences (Jain et al., 2002), (ii) the assessment of erosion controlling factors (King et al., 2005; Vrieling et al., 2008), and (iii) the interpretation and

* Corresponding author. Tel./fax: +1 514 398 7786.
E-mail address: jan.adamowski@mcgill.ca (J. Adamowski).

0341-8162/$ – see front matter © 2013 Elsevier B.V. All rights reserved.
http://dx.doi.org/10.1016/j.catena.2013.08.012

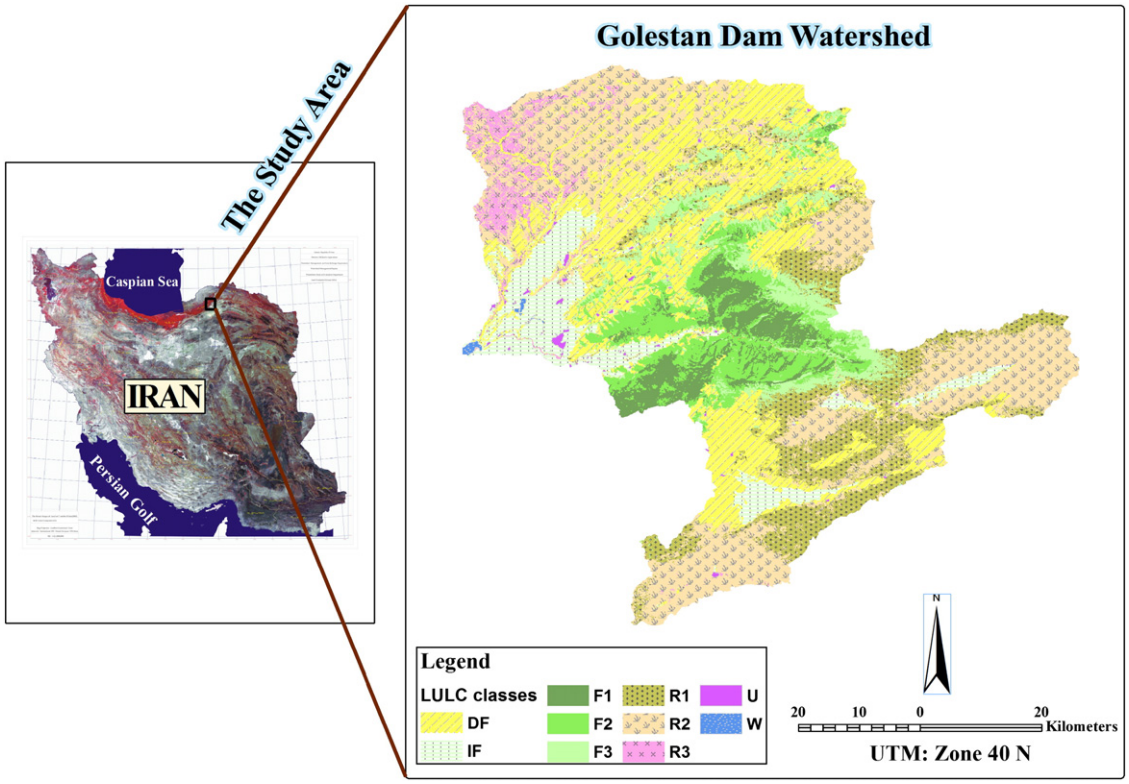

Fig. 1. Location of the study area.

classification of soil erosion using satellite data combined with additional data sources (ancillary layers).

In the first case, where high-resolution satellite data are used, large-scale erosion types (e.g. gully and badland) can be identified automatically from the satellite data. In the second case, a variety of erosion controlling factors such as vegetation, topography, climate, and soil characteristics can be obtained from satellite imagery (King et al., 2005). These data can then be used in a range of empirical models, leading to the quantitative assessment of small-scale erosion features. For instance, the empirical Universal Soil Loss Equation (USLE) can be used, in which long-term mean interrill and rill erosions are assessed (Wischmeier and Smith, 1978). Similarly, the USLE, its revised (RUSLE) and modified (MUSLE) versions (Renard et al., 1997; Smith et al., 1984), the Water Erosion Prediction Program (WEPP) (Flanagan et al., 2001), and the European Soil Erosion Model (EUROSEM) (Morgan, 1995; Morgan et al., 1984) can be used in which erosion controlling factors extracted from satellite data at basin or even regional scales play a role in assessing/mapping erosion intensities (de Vente and Poesen, 2005). The development of such models based on these factors is problematic as a number of these factors are difficult to be assessed, and are not constant in space and time and interact with each other (de Vente and Poesen, 2005). In addition, fixed data requirements, and the fact that these models are developed for a certain region, scale, or specific process and that they only provide a mean quantitative assessment of erosion phenomena, are drawbacks to their general use (Rudra et al., 1998; Vrieling, 2006). Although outputs of such models are helpful in prioritizing conservation projects within a watershed, they cannot provide detailed information of map erosion features (Poesen et al., 2003).

In the third case, erosion types/intensities can be differentiated using satellite data combined with some ancillary layers (Dymond et al., 2002; Focardi et al., 2008; Healey et al., 2005; Vrieling et al., 2008). Remote sensing data provides detailed information over large regions with a regular revisit capability, and can greatly contribute to regional erosion assessment (Siakeu and Oguchi, 2000; Vrieling et al., 2008). For instance, Liberti et al. (2008) mapped badland areas using landsat TM/ETM satellite imagery with the aid of some morphological maps. Vrieling et al. (2008) created soil erosion risk maps using a time series of MODIS (Moderate Resolution Imaging Spectroradiometer) and ASTER (Spaceborne Thermal Emission and Reflection Radiometer) images plus a digital elevation model (DEM) and temporal rainfall data. They reported a strong relationship between the normalized difference vegetation index (NDVI) and erosion risk. However, most approaches using remotely sensed data have concentrated on mapping large-scale erosion features (e.g. gullies) and erosion risk (King et al., 2005), but little has been done with regard to creating maps showing the erosion intensity classes over the land surface by interrill and rill processes (de Vente et al., 2008). It should also be noted that medium resolution satellite data alone cannot provide appropriate information for mapping small scale erosion features like interrill and rill (Alewell et al., 2008; Vrieling, 2006). A review of existing approaches for erosion types/intensities mapping shows that although the application of high-resolution satellite images (e.g. QuickBird, GeoEye and IKONOS) may lead to very accurate soil erosion type/intensity maps, these data are not accessible for all countries (such as the study area of this project: Iran), and are very expensive if used at the regional and national scales. Thus, it can be seen that there is a gap in the literature and in practice for methods with the capability of creating soil erosion maps (particularly small scale soil erosion features) that use medium resolution satellite images at the regional and national scales (Vrieling, 2006).

The principal objective of the present study is to investigate the applicability of the brightness index (Tasseled Cap) variation over the growing season to generate accurate interrill and rill erosion intensity maps using medium resolution satellite images and some ancillary layers at a regional level.

2. The study area

With an area of 4511.8 km^2, Iran's Golestan dam watershed is located between 55° 21′ and 56° 28′ E longitude, and 36° 44′ and 37° 49′ N

latitude, in the northeast portion of the Golestan province (Fig. 1). This sub-watershed of the Gorgan River watershed is a complex combination of mountains, hills, plains and rivers. The highest elevation is 2492 m above mean sea level and the lowest is 47 m. Because of its geographic situation and topography, a wide range of climates prevail across the different portions of the watershed; from semi-arid in the north-west and south to humid in the central portion. Mean annual precipitation ranges from 135 mm to 700 mm and mean annual air temperature from 8.5 to 17 °C. March is the month of greatest rainfall and June to October are the dry months. Different sedimentary rocks such as limestone, sandstone, shale, dolomite, and marl, along with conglomerate, loess sediments and alluvium cover the area (Lar Consulting Engineering, 2007).

Existing land use and land cover (LULC) maps show that rangeland covers an area of 200,315 ha (44.4% of the whole study area), forest an area of 98,521 ha (21.83%), dryland farming an area of 110,135 ha (24.41%), irrigated farming an area of 39,068 ha (8.66%), with urban areas contributing less than 1% (Saadat et al., 2011). Located in this area, the 92,000 ha Golestan Forest National Park is recognized by UNESCO as part of the international network of Biosphere Reserves (Japan International Cooperation Agency, 2005). Accelerated soil erosion, high sediment yields, floods and debris flows are serious problems in the Golestan dam watershed (Japan International Cooperation Agency, 2005). For example, close to 500 people were killed, thousands of livestock were lost and many infrastructures such as bridges and roads were washed out or damaged due to flooding and debris flows during the summers of 2001, 2002 and 2005 (Japan International Cooperation Agency, 2005; Sharifi et al., 2002).

3. Materials and methods

3.1. Materials

To implement the research methodology, the following data, image and map materials are required:

(i) Growing season Landsat ETM+ images: spring (10 May, 2003), summer (10 July, 2002), and late-summer (12 September, 2002); with 28.5 m spatial resolution in multispectral bands.
(ii) 1:25000 digital topographic maps prepared (based on 1993 aerial photos) by the National Cartographic Center of Iran and the Forest, Range and Watershed Management Organization.
(iii) Three digital ancillary layers to assist the production of homogeneous land units. These layers consist of a 1:25000 scale slope (LS) map (Saadat et al., 2008), a 1:50000 scale landform (LF) map (Saadat et al., 2008), and a 1:50000 scale land use and land cover (LULC) map (Saadat et al., 2011). The legend classification for the slope, landform, and land use land cover maps can be found in the footnotes on the next page.
(iv) ERDAS Imagine (version 8.7) and ArcInfo (version 9) software are used for image processing and data analyses.

3.2. Methodology

As previously mentioned, the principal objective of this research work is to map intensity of interrill and rill erosions using the brightness variation over the growing season in a large-scale watershed. To do that, five main steps are proposed (Fig. 2a, b, and c).

3.2.1. Preprocessing of satellite images

The 6 bands of each ETM+ images (except thermal bands) were stacked. These images have their own map projection according to orbital parameters but to be able to compare separate images pixel by pixel, the pixel grids of each image must conform to the other images in the data base. The September stacked image using 160 ground control points taken from 1:25000 topographic maps is geometrically corrected. The total RMS Error (distance in pixel widths) in this stage was equal to 0.8 and the first polynomial order was used in order to have less distortions. At the next stage the other two stacked images are registered to the September image (Fig. 2a. operations 1 and 2).

3.2.2. Ground-truth sampling locations

This step aims to determine an appropriate number and location of sampling points over the study area, at which the degree of interrill and rill erosions is measured. The number and location of the sampling points should be specified in a way that entails the full range of erosion intensities in any possibility of land configuration (e.g. slope, land use and landform). To do that, three ancillary layers, including slope with 9 classes,[1] landform with 7 classes[2] and land use land cover with 8 classes,[3] is overlayed on each other in order to generate a Homogeneous Land Unit (HLU) map (Fig. 2c, operations 8 and 9). In this case study, the HLU map contains 147 unique units. Since each driven unit has similar characteristics of erosion controlling factors (similar land form, slope, land use and vegetation density), this map was used in an important supportive role for identifying appropriate sampling locations across the entire study area (de Vente and Poesen, 2005).

Using the stratified random sampling technique (Stehman, 1999), a total of 1328 ground control points over the entire study area were initially extracted. Nineteen of these sites are inaccessible due to physical barriers or remoteness from roads, and inevitably omitted from the sampling points list. These sites are replaced by 19 additional accessible sites with the same attributes. Erosion type information collected at the 1328 locations are divided into training and reference data sets. The training data set consists of the 50% collected points (664 points) that are used in the training process and the rest are treated for accuracy assessment process of soil erosion intensity classification.

3.2.3. Field assessment of interrill and rill erosions

This step aims to collect the ground-truth interrill and rill erosion severity data at the sampling locations. A topographic map (1:25000) and a GPS unit are used to locate each site. Based upon the handbook provided by Stocking and Murnaghan (2001) for the field assessment of land degradation, a number of indicators are selected to determine the degree of interill and rill erosions in an area around the sampling location equal to 1 to 3 image pixels. Since ETM+ multispectral bands were used in this study, then based on their pixel size, the plot area was considered to be approximately between 30 * 30 and 90 * 90 m (Fig. 2c, operation 10). These severity indicators include: a) soil color condition, b) plant and tree root exposure, c) build-up against tree trunk/plant stem of soil and/or plant debris, d) rock outcrops or stony soil surface, e) presence, depth and length of rills, and f) distance between rills.

In order to establish a measure of interrill and rill erosion severity, Table 1 is generated using the considered severity indicators and a combination of the methods provided by FAO (2006), Morgan (2005), and Stocking and Murnaghan (2001). According to the collected ground-truth data at the sampling locations, fifteen erosion types are identified, as illustrated in the matrix of Table 2 (Fig. 2c, operation 11).

3.2.4. Assessment of brightness index variation

As previously mentioned, the main objective of this research is to determine interrill and rill erosion intensity using the brightness index variation over a growing season. Therefore, the Tasseled Cap transformation technique is initially performed on each image to determine

[1] Slope classes include <2%, 2–5%, 5–8%, 8–12%, 12–15%, 15–25%, 25–40%, 40–60%, and ≥60%.
[2] Landform classes contain River Alluvial Plains (RP), Piedmont Plains (PD), Gravelly Fans (GF), Upper Terraces (TRu), River Terraces (TRr), Hills (H) and Mountains (M).
[3] Land use and land cover classes include Irrigated Farming (IF), Dryland Farming (DF), high density Forest (F1, cover > 70%), medium density Forest (F2, 40% < cover ≤ 70%), low density Forest (F3, cover ≤40%), high density Rangeland (R1, cover > 30%, mostly between 30% and 50%), medium density Rangeland (R2, 15 < cover ≤ 30%), and low density Rangeland (R3, cover ≤ 15%).

the value of brightness index (Fig. 2b. operations 4, 5, 6, and 7). The technique reduces the six ETM+ reflectance bands of a single image to three individual indices termed brightness, greenness, and wetness. These three individual indices are derived using at-satellite reflectance based coefficients (Huang et al., 2002). The use of the DN (digital number) based transformation in multiscene applications can be problematic, because changing sun illumination geometry strongly affects DN, and thus affects the derived Tasseled Cap value. However, a large part of the impact of illumination geometry can be normalized by converting DN to at satellite reflectance. Therefore, a transformation based on at-satellite reflectance is more appropriate for regional applications where atmospheric correction is not feasible (Crist and Kauth, 1986).

The difference in the values of brightness is computed for each pixel by subtracting the values of one imaging date from the next. To be specific, the May brightness value is subtracted from the July one, termed as the B_{MJ} image, and the July brightness value is subtracted from the September one, termed as the B_{JS} image. In each interval period, the difference in the value of brightness of each pixel may decrease, increase, or remain unchanged, termed as D, I and C, respectively. Hence, the attribute of each pixel in the B_{MJ} and B_{JS} images can take terms D, I and C.

The B_{MJ} and B_{JS} images are combined to get a unique attribute table representing the trend of the brightness index variation over the May–July and July–September intervals, respectively. The resultant image contains 7 classes including DD (the brightness values decreases over both interval periods), DI (the brightness values decreases over the May–July interval and increases over the July–September interval), DC (the brightness values decreases over the first interval period and that

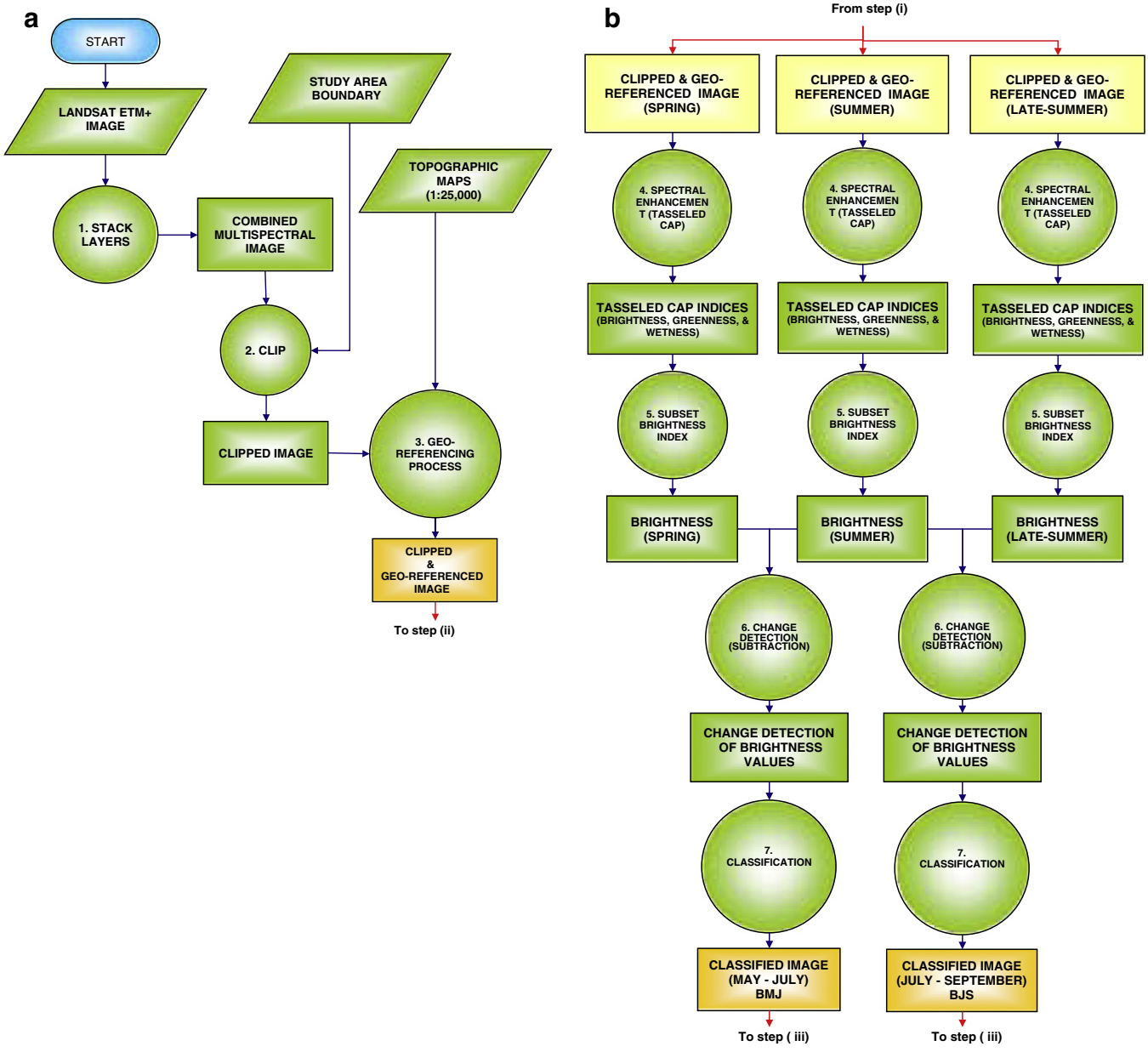

Fig. 2. Processing steps for (a) preprocessing of the images, (b) applying Tasseled Cap transformation, (c) extracting homogeneous land units and sampling location map, field data collection, analysis and classification, extending and identifying soil erosion intensities. Circles = operation, trapezoids = data input, and rectangles = maps or coverages.

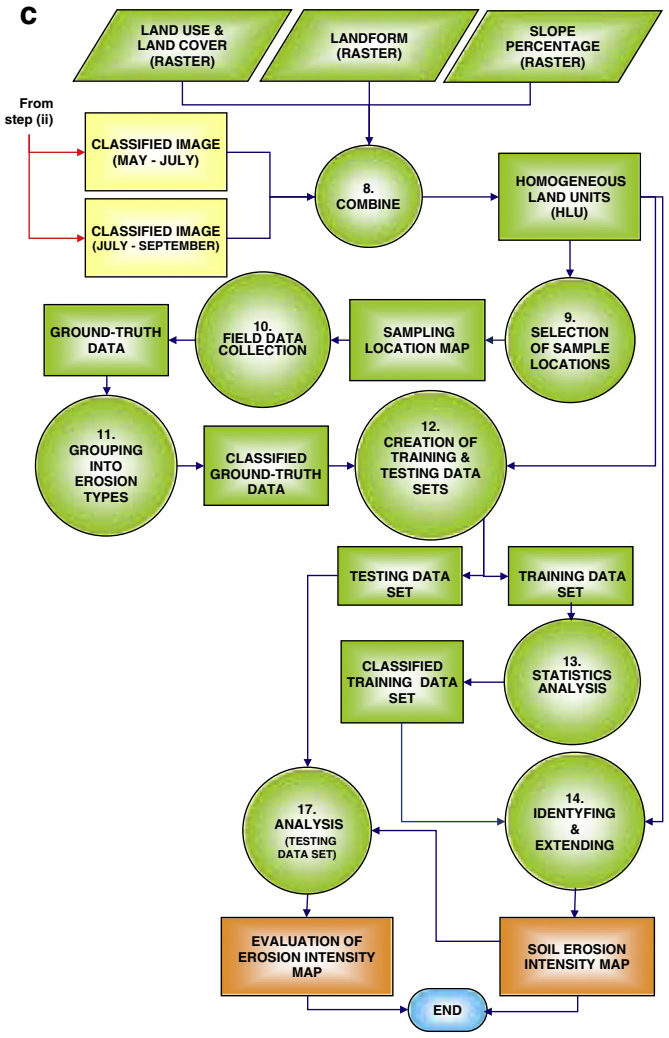

Fig. 2 (*continued*).

the brightness values remains unchanged over the second interval), II, IC, CI and CC.

3.2.5. Brightness changes and erosion intensity relationship

In order to increase the chance to make a logical relation between the trend of brightness index variation and interrill–rill erosion types, the 15 interrill–rill erosion types are subsequently grouped into five categories (five erosion intensities[4]) as shown in Table 2. The five categories comprise slight erosion intensity (E_S), moderate erosion intensity (E_M), high erosion intensity (E_H), severe erosion intensity (E_{SE}), and very severe erosion intensity (E_{VSE}). Based on the collected ground-truth data at the sampling locations, a database is created for all 1328 field sites, such that each site is assigned one of five interrill–rill erosion intensities (Table 3).

Using the erosion intensities and the B_{MJ} and B_{JS} trends at the training sampling points, a logical relationship is found between them (Table 3). Based on this relationship, the erosion intensity of each HLU polygon can be derived based on the trend of the brightness value variation and zonal analysis. For instance, in Table 3, one can see that given the trend of the brightness index variation over the two growing season intervals (i.e. B_{MJ} and B_{JS}) is DI, one can expect high erosion intensity (i.e. E_H) at the HLU of interest. To assess the accuracy of the established relationship, it is applied on all HLUs over the study area to derive the erosion intensity at each HLU.

4. Accuracy assessments

Using the error matrix method (Congalton, 1991), the accuracy of the method is assessed using a different set of 50% referenced points. This is done only in forest and rangeland areas (Table 4). As mentioned earlier, the capability of the proposed method is only assessed in forest (F) and rangeland (R) land uses since the established logical relationship between the erosion intensities and the B_{MJ} and B_{JS} trends is not found in other land uses due to anthropogenic effects in them.

5. Results and discussion

Considering only rangeland (R) and forest (F) land uses, a logical relationship exists between the interrill–rill erosion intensity of each HLU and the trend of the brightness index variation. For example, as seen in Table 3, in the case of the slight interrill–rill erosion intensities (E_S) the trend of the brightness index variation over the two growing season intervals is DD, excluding rocky areas of more than 80% outcrop (RO_D) which is CC. In the case of E_M, E_H, E_{SE} and E_{VSE} the trends of the brightness index variation are DC, DI, CI and II, respectively. This means that by having the brightness index trend change over the two growing season intervals, interrill–rill erosion intensities can be determined at each HLU where land use is either forest or rangeland. Having determined interrill–rill erosion intensities, an interrill–rill soil erosion intensity map can then be generated for the study area (Fig. 3).

Such a direct relationship does not exist for other land uses (i.e. IF and DF), most likely due to a masking effect associated with the greater degree of anthropogenic activities within these land uses. Irrigated farming (IF) and dryland farming (DF) both experience much more anthropogenic land alteration than rangeland (R) and forest (F). This anthropogenic alteration of IF and DF tends to mask, or remove to a large degree, evidence of rill and interrill erosions, and so changes in brightness are not a result of natural rill or interrill development but of anthropogenic alterations.

Considering only R and F and excluding RO_D land uses, for the lower erosion intensities (E_S, E_M and E_H), all have a brightness trend of D in the first interval. As erosion intensities move from E_S to E_M and then to E_H, the brightness trend goes from D to C, and then to I in the second interval, respectively. Even though spring rains cause the development of rill and interrill features, increasing vegetation growth in the early season masks this and the net impact is a brightness trend of D in the first interval for all three lower erosion intensities (E_S, E_M and E_H). Subsequently, as summer progresses with little rain, vegetative cover decreases. For E_S where less than 5% of the HLU area experiences erosion, vegetation is still dense enough to mask the erosion and the brightness trend continues as D. For E_M where between 5 and 10% of the HLU area is eroded, vegetative cover is less effective and the brightness trend becomes C. Finally, for E_H where 10 to 25% the HLU area is eroded, vegetative cover is even less effective and the brightness trend changes to I. As such, for the lower erosion intensity ranges, it is the brightness trend in the second interval of the growing season (B_{JS}) which determines the degree of erosion intensity among E_S, E_M, and E_H.

For the areas of severe and very severe erosion intensity (i.e. E_{SE} and E_{VSE}), changes in the brightness trend is also evident. In the case of E_{SE} and E_{VSE}, the brightness trend in the first interval is C and I, respectively, while the brightness trend in the second interval for both cases remains unchanged as I. In these cases, vegetative cover masks erosion

[4] Slight erosion intensity (E_S, less than 5% of soil area affected by interill and rill erosion), moderate erosion intensity (E_M, 5 to 10% of soil area affected by interill and rill erosion), high erosion intensity (E_H,10 to 25% of soil area affected by interill and rill erosion), severe erosion intensity (E_{SE}, 25 to 50% of soil area affected by interill and rill erosion) and very severe erosion intensity (E_{VSE}, more than 50% of soil area affected by interill and rill erosion).

Table 1
Means of establishing severity of interrill and rill erosion.

Feature of erosion	Degree	Description
Interrill erosion (S)	Not apparent (S0)	No obvious signs of interrill erosion.
	Slight (S1)	No evidence of plant root exposure but in less than 5% of the area plant debris or/and topsoil particles removed from their original location through surface wash. Soil level slightly higher on upslope of plants and boulders. At some locations the surface is covered by more than 80% rock outcrops (RO_D) and only less than 5% of the soil surface is affected by interrill erosion (S1 + RO_D).
	Moderate (S2)	Plant debris or/and topsoil particles removed from their original location through surface wash in 5 to 10% of the area. Most of these particles are deposited on the upslope side of plant stems with a height of 5–10 mm and plant roots are partially exposed above the present soil surface with a height of 5–20 mm. S2 is usually restricted to areas with no rill to high rill erosion, depending on the land s lope. At some locations the surface is covered by 40–80% rock outcrops (RO_A) and just 5 to 10% of the soil surface is affected by interrill erosion (S2 + RO_A).
	High (S3)	Plant debris and topsoil particles removed through surface wash in 10 to 25% of the area. Heavier particles are deposited on the upslope side of plant stems with a height of 10–30 mm and plant roots are partially exposed above the present soil surface with a height of 20–50 mm. S3 is usually restricted to areas with moderate to severe rill erosion (Ri2, Ri3, or Ri4).
	Severe (S4)	Topsoil particles transported through surface wash in 25 to 50% of the area. Heavier particles are deposited on the upslope side of plant stems with a height of 30–50 mm and plant roots are partially exposed above the present soil surface over 50 mm high. S4 is usually restricted to areas with high to very severe rill erosion (Ri3 or Ri5).
	Very severe (S5)	Most (>50%) of the original soil surface removed and subsoil horizons exposed at or close to the soil surface. Accumulation of soil on the upslope side of plants and boulders are over 50 mm high. Extensive exposure of plant roots occurred in more than 50% of the area. S5 is usually restricted to areas with severe rill erosion (Ri4).
Rill erosion (Ri)	Not apparent (Ri0)	No rills present.
	Slight (Ri1)	A few shallow rills, less than 10 cm depth spaced every 20–50 m, which are able to transport soil particles from their original location. Ri1 is always associated with S1 or S2.
	Moderate (Ri2)	Discontinuous rills, less than 15 cm depth spaced every 10–20 m. Plant debris and soil particles are transported via runoff. Ri2 is usually associated with S2, and in some areas where slope is over 8%, with S3.
	High (Ri3)	A continuous network of shallow to moderately deep rills (less than 20 cm depth) spaced every 5–10 m. Soil particles, even heavier particles are transported and deposited long distances. Ri3 is usually associated with S2, S3, or S4 depending on vegetation cover and slope.
	Severe (Ri4)	A continuous network of deep rills (up to 30 cm depth) spaced every 2–5 m. Most of the original soil surface is removed. Ri4 is always associated with S3, S4 or S5 depending on LULC and slope.
	Very severe (Ri5)	An extensive network of rills spaced less than 2 m. Most of the original soil surface removed. Ri5 is usually associated with S4.

development to a lesser degree compared to lower erosion intensities. As seen in Table 3, the brightness trend in the first interval of the growing season (B_{MJ}) is a determinant of E_{SE} and E_{VSE}.

Table 2
Grouping interill and rill erosions into erosion type and intensity.

Rill / Interrill	Ri0 (Not apparent)	Ri1 (Slight)	Ri2 (Moderate)	Ri3 (High)	Ri4 (Severe)	Ri5 (Very severe)
S0 (Not apparent)	-	-	-	-	-	-
S1 (Slight)	S1 (E_S)	S1Ri1 (E_S)	-	-	-	-
S1+RO_D (Slight)	-	S1Ri1+RO_D (E_S)				
S2 (Moderate)	S2 (E_M)	S2Ri1 (E_M)	S2Ri2 (E_M)	S2Ri3 (E_H)	-	-
S2+RO_A (Moderate)	-	S2Ri1+RO_A (E_M)	S2Ri2+RO_A (E_M)	-		
S3 (High)	-	-	S3Ri2 (E_H)	S3Ri3 (E_H)	S3Ri4 (E_{SE})	-
S4 (Severe)	-	-	-	S4Ri3 (E_{SE})	-	S4Ri5 (E_{VSE})
S5 (Very severe)	-	-	-	-	S5Ri4 (E_{VSE})	-

E_S:	Slight erosion intensity (less than 5% of soil area affected by erosion)	E_M:	Moderate erosion intensity (5 to 10% of soil area affected by erosion)	E_H:	High erosion intensity (10 to 25% of soil area affected by erosion)
E_{SE}:	Severe erosion intensity (25 to 50% of soil area affected by erosion)	E_{VSE}:	Very severe erosion intensity (more than 50% of soil area affected by erosion)		

RO_A: surface cover of rock outcrops is 40–80%.
RO_D: surface cover of rock outcrops is more than 80%

Using 531 referenced sites and the method of Congalton (1991), the interrill–rill erosion intensity for each of the testing ground-truthing points was evaluated (Table 4). An overall accuracy of 96% was achieved. The producer's accuracy (PA) is a measure of how correct the classification is. As shown in Table 4, the PA ranged from a low of 92.3% in the case of E_{SE} to a high of 98% in the case of E_S. The user's accuracy (UA) is a measure of how well the classification process captures all occurrences of any of the five erosion intensity types. In this study, the UA ranged from a low of 92.3% in the case of E_{SE} to a high of 98% in the case of E_M.

Based on the proposed method, the interrill–rill erosion intensities of all HLUs across the study area using the trend of brightness index

Table 3
The 15 erosion types and their corresponding descriptive combinations of B_{MJ} and B_{JS}.

Erosion types[1]	B_{MJ}[2]	B_{JS}[2]	E[3]
S1	D	D	E_S
S1Ri1	D	D	
S1Ri1 + RO_D[4]	C	C	
S2	D	C	E_M
S2Ri1	D	C	
S2Ri2	D	C	
S2Ri1 + RO_A[4]	D	C	
S2Ri2 + RO_A	D	C	
S2Ri3	D	I	E_H
S3Ri2	D	I	
S3Ri3	D	I	
S3Ri4	C	I	E_{SE}
S4Ri3	C	I	
S4Ri5	I	I	E_{VSE}
S5Ri4	I	I	

[1] The 15 erosion types as determined by ground-truth data.
[2] B_{MJ}: classes derived by subtracting May (spring) brightness from July (summer) brightness and B_{JS}: classes derived by subtracting July brightness from September (late-summer) brightness; with the result that some of these values decreased (D), some increased (I), and the others remained without changing (C).
[3] E: interrill and rill erosion intensities, E_S: slight erosion intensity, E_M: moderate erosion intensity, E_H: high erosion intensity, E_{SE}: severe erosion intensity, and E_{VSE}: very severe erosion intensity.
[4] RO_D: surface cover of rock outcrops is more than 80% and RO_A: surface cover of rock outcrops is 40–80%.

Table 4
Testing data set error matrix of classification process.

Interrill–rill erosion intensities	Ground-truth data					New classified	User's accuracy %
	E_S	E_M	E_H	E_{SE}	E_{VSE}		
E_S	150	7	0	0	0	157	95.5
E_M	3	195	1	0	0	199	98
E_H	0	0	68	3	0	71	95.8
E_{SE}	0	0	3	60	2	65	92.3
E_{VSE}	0	0	0	2	37	39	94.9
Total sites visited	153	202	72	65	39	531	
Producer's accuracy %	98	96.5	94.4	92.3	94.9		
Overall classification accuracy = 96%							

change over the two intervals of growing season is determined. This means that by applying this method over the study area, an interrill–rill erosion intensity map is created. To further verify the credibility of this method in creating such a map, the consistency between the attributes (i.e. land use, land cover and slop) belonging to each class of erosion intensity over the whole study site is studied. To do that, these attributes are firstly extracted from the produced soil erosion intensity map (see Table 5). As seen in Table 5, as erosion intensity increases (from E_s toward E_{vse}), land use changes from high density forests to poor rangelands. Similarly, as erosion intensity increases (from E_s toward E_{vse}), land slope increases except in high and medium density forests (F1 and F2). F1 and F2 are correctly classed as erosion intensity type E_s, even in areas of steep and very steep slopes. These shows that there is a consistency between the attributes of each class of erosion intensity, and corroborates other research (de Vente et al., 2008; Kimaro et al., 2008; King et al., 2005; Liberti et al., 2008) that has found that land use, land cover, and land slope play an important role in governing erosion.

Table 5
The five interrill–rill erosion intensities and their corresponding descriptive combinations of B_{MJ}, B_{JS}, LULC and LS.

E[1]	Erosion TYPES[2]	B_{MJ}[3]	B_{JS}[3]	LULC[4]	LS %[5]
E_S	S1	D	D	F1, F2	<60
	S1Ri1	D	D	F3	<60
	S1Ri1	D	D	R1, R2	<60
	S1Ri1 + RO_D[6]	C	C	F2	>40
	S1Ri1 + RO_D[6]	C	C	R2, R3	>40
E_M	S2	D	C	R2, R3	0–2
	S2Ri1	D	C	F3	<15
	S2Ri1	D	C	R1, R2, R3	2–5
	S2Ri2	D	C	R1, R2, R3	5–8
	S2Ri1 + RO_A[6]	D	C	R1, R2, R3	>12
	S2Ri2 + RO_A	D	C	F3	>15
E_H	S2Ri3	D	I	R1, R2	8–12
	S3Ri2,	D	I	R2, R3	8–25
	S3Ri3	D	I	R1, R2, R3	>25
E_{SE}	S3Ri4	C	I	R2, R3	12–25
	S4Ri3	C	I	R2, R3	>15
E_{VSE}	S4Ri5	I	I	R3	>25
	S5Ri4	I	I	R2, R3	>15

[1] Interrill–rill erosion intensities (E): slight erosion intensity (E_S), moderate erosion intensity (E_M), high erosion intensity (E_H), severe erosion intensity (E_{SE}), and very severe erosion intensity (E_{VSE}).
[2] The 15 erosion types as determined by ground-truth data.
[3] RO_D: surface cover of rock outcrops is more than 80% and RO_A: surface cover of rock outcrops is 40–80%.
[4] B_{MJ}: classes derived by subtracting May (spring) brightness from July (summer) brightness and B_{JS}: classes derived by subtracting July brightness from September (late-summer) brightness; with the result that some of these values decreased (D), some increased (I), and the others remained without changing (C).
[5] For land use and land cover (LULC) map ten classes were used (Saadat et al., 2011): irrigated farming (IF), dryland farming (DF); forest (F): high density forest (F1, cover > 70%), medium density forest (F2, 40% < cover ≤ 70%), and low density forest (F3, cover ≤ 40%); rangeland (R): high density rangeland (R1, cover > 30%, mostly between 30% and 50%), medium density rangeland (R2, 15 < cover ≤ 30%), and low density rangeland (R3, cover ≤ 15%); urban (U), and water bodies (W).
[6] LS: land slope.

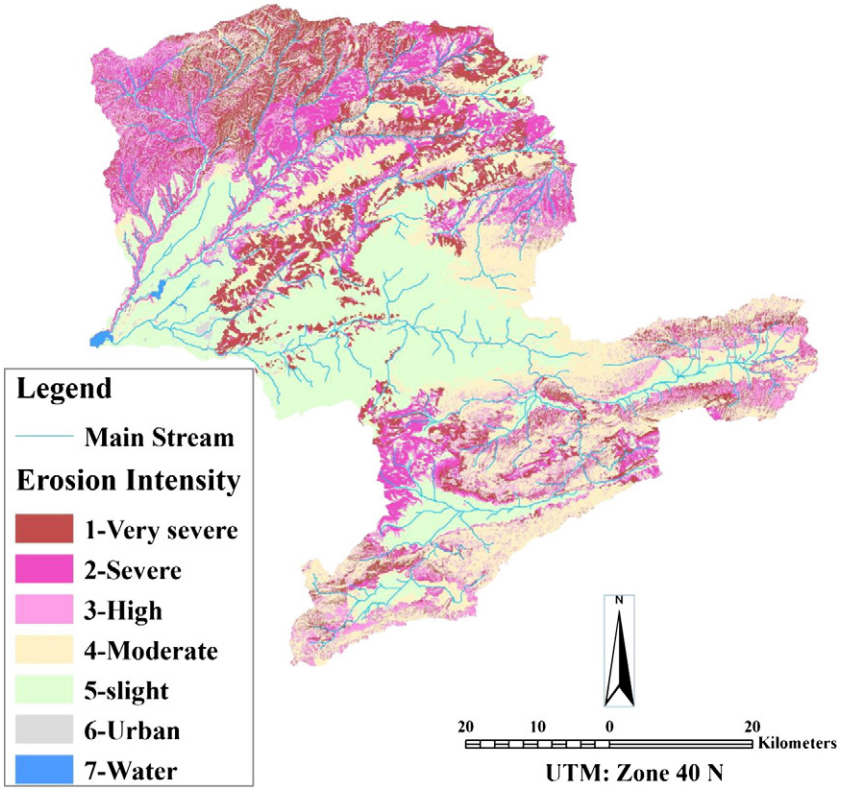

Fig. 3. Soil erosion intensities map.

6. Conclusions and recommendations

This study encompassed a relatively large watershed (4511.8 km^2) which included a variety of erosion types/intensities, from slight to very severe. More than 24% of the land surface experiences severe and very severe erosion. The original contribution of this study is the inclusion of a brightness index (B_{MJ} and B_{JS}) in order to enhance interrill–rill erosion intensity classification. Considering only rangeland and forest (66.2% of the total area), for each interrill–rill erosion intensity it was found that a unique combination of brightness occurred.

The newly proposed approach presented in this paper is expected to be a powerful tool in the creation of interrill–rill erosion intensity maps over large areas, which in turn can be used in the development of soil conservation and watershed management plans, especially in regions with limited high resolution image access and limited accurate data of erosion controlling factors such as vegetation, topography, climate, and soil characteristics. The unique advance made during the development of this protocol is the application of medium resolution satellite images in combination with some ancillary layers to create interrill–rill erosion intensity maps with an accuracy of 96%. It is recommended that further research similar to that presented in this paper be conducted in other regions with differing climatic and geomorphologic characteristics to show whether the proposed protocol presented in this paper can be used effectively in other areas. The analysis as presented in this paper could also be done with satellite images taken at different times of the season. It may be, particularly for other climatic zones, that there is a better time of season for image acquisition that would provide more information. In addition, atmospheric correction is another approach that could be explored in future studies to improve the accuracy of image classifications. This was not explored in this study; however, this is a promising topic for future research.

Acknowledgments

The authors gratefully acknowledge the Forest, Range and Watershed Management Organization of Iran and the Watershed Management Office of Golestan Province for providing available datasets and facilities, manpower and field support for this study. Partial funding for this study came from a grant held by Jan Adamowski from the Natural Sciences and Engineering Research Council of Canada.

References

Alewell, C., Meusburger, K., Brodbeck, M., Banninger, D., 2008. Methods to describe and predict soil erosion in mountain regions. Landsc. Urban Plan. 88, 46–53.
Congalton, R.G., 1991. A review of assessing the accuracy of classifications of remotely sensed data. Remote. Sens. Environ. 37, 35–46.
Consulting Engineering, Lar, 2007. The study on flood and debris flow in the Golestan province. Regional Water Board in Golestan. Ministry of Energy, Tehran, Iran (425 pp. (In Farsi)).
Crist, E.P., Kauth, R.J., 1986. The tasseled cap de-mystified. Photogramm. Eng. Remote. Sens. 52 (1), 81–86.
de Vente, J., Poesen, J., 2005. Predicting soil erosion and sediment yield at the basin scale: scale issues and semi-quantitative models. Earth Sci. Rev. 71, 95–125.
de Vente, J., Poesen, J., Verstraeten, G., Van Rompaey, A., Govers, G., 2008. Spatially distributed modelling of soil erosion and sediment yield at regional scales in Spain. Glob. Planet. Chang. 60, 393–415.
Dymond, C.C., Mladenoff, D.J., Radeloff, V.C., 2002. Phenological differences in Tasseled Cap indices improve deciduous forest classification. Remote. Sens. Environ. 80, 460–472.
FAO, 2006. Guidelines for Soil Description. Food and Agriculture Organization of the United Nations, Rome (97 pp.).
Flanagan, D.C., Ascough II, J.C., Nearing, M.A., Laflen, J.M., 2001. The water erosion prediction project (WEPP) model. In: Harmon, R.S., Doe III, W.W. (Eds.), Landscape Erosion and Evolution Modeling. Kluwer Academic/Plenum Publishers, New York, pp. 145–199.
Focardi, S., Loiselle, S.A., Mazzuoli, S., Bracchini, L., Dattilo, A.M., Rossi, C., 2008. Satellite-based indices in the analysis of land cover for municipalities in the province of Siena, Italy. J. Environ. Manag. 86, 383–389.
Healey, S.P., Cohen, W.B., Zhiqiang, Y., Krankina, O.N., 2005. Comparison of Tasseled Cap-based Landsat data structures for use in forest disturbance detection. Remote. Sens. Environ. 97, 301–310.
Huang, C., Wylie, B., Yang, L., Homer, C., Zylstra, G., 2002. Derivation of a tasseled cap transformation based on Landsat 7 at-satellite reflectance. Int. J. Remote. Sens. 23 (8), 1741–1748.
Jain, S.K., Singh, P., Seth, S.M., 2002. Assessment of sedimentation in Bhakra Reservoir in the western Himalayan region using remotely sensed data. Hydrol. Sci. J. 47 (2), 203–212.
Japan International Cooperation Agency (JICA), 2005. The study on flood and debris flow in the Caspian Coastal area focusing on the flood-hit region in Golestan province. Interim Report (Tehran, Iran, 302 pp.).
Kimaro, D.N., Poesen, J., Msanya, B.M., Deckers, J.A., 2008. Magnitude of soil erosion on the northern slope of the Uluguru Mountains, Tanzania: interrill and rill erosion. Catena 75, 38–44.
King, C., Baghdadi, N., Lecomte, V., Cerdan, O., 2005. The application of remote sensing data to monitoring and modelling of soil erosion. Catena 62, 79–93.
Liberti, M., Simoniello, T., Carone, M.T., Coppola, R., D'Emilio, M., Macchiato, M., 2008. Mapping badland areas using LANDSAT TM/ETM satellite imagery and morphological data. Geomorphology. http://dx.doi.org/10.1016/j.geomorph.2008.11.012.
Morgan, R.P.C., 1995. Soil Erosion and Conservation. Longman Group Limited, Essex, UK (198 pp.).
Morgan, R.P.C., 2005. Soil Erosion and Conservation, 3rd edition. Blackwell publishing, Oxford (304 pp.).
Morgan, R.P.C., Morgan, D.D.V., Finney, J.J., 1984. A predictive model for the assessment of erosion risk. J. Agric. Eng. Res. 30 (3), 245–253.
Parsons, A.J., Wainwright, J., 2006. Depth distribution of interrill overland flow and the formation of rills. Hydrol. Processes 20 (7), 1511–1523.
Poesen, J., Nachtergaele, J., Verstraeten, G., Valentin, C., 2003. Gully erosion and environmental change: importance and research needs. Catena 50 (2), 91–133.
Renard, K.G., Foster, G.R., Weesies, G.A., McCool, D.K., Yoder, D.C., 1997. Predicting soil erosion by water: a guide to conservation planning with the revised universal soil loss equation (RUSLE). Agriculture Handbook. vol. 703. US Department of Agriculture, Washington DC (384 pp.).
Rudra, R.P., Dickinson, W.T., Wall, G.J., 1998. Problems regarding the use of soil erosion models. In: Boardman, J., Favis-Mortlock, D. (Eds.), Modelling Soil Erosion by Water. Proceedings of the NATO, Global Environmental Change, vol. 55. Springer, Berlin, pp. 175–189.
Saadat, H., Bonnell, R., Sharifi, F., Mehuys, G., Namdar, M., Ale-Ebrahim, S., 2008. Landform classification from a digital elevation model and satellite imagery. Geomorphology 100, 453–464.
Saadat, H., Adamowski, J., Bonnell, R., Sharifi, F., Namdar, M., Ale-Ebrahim, S., 2011. Land use and land cover classification over a large area in Iran based on single date analysis of satellite imagery. ISPRS J. Photogramm. Remote Sens. 66 (5), 608–619.
Sharifi, F., Saghafian, B., Telvari, A., 2002. The great 2001 flood in Golestan province, Iran: causes and consequences. Proceedings of the International Conference on Flood Estimation. March 6–8, 2002. Berne, Switzerland, CHR-KHR Report 11–17, pp. 263–271.
Siakeu, J., Oguchi, T., 2000. Soil erosion analysis and modelling: a review. Trans. Jpn. Geomorphol. 21 (4), 413–429.
Smith, S.J., Williams, J.R., Menzel, R.G., Coleman, G.A., 1984. Prediction of sediment yield from Southern Plains grasslands with the Modified Universal Soil Loss Equation. Journal of Range Management 37 (4), 295–297.
Stehman, S.V., 1999. Basic probability sampling designs for thematic map accuracy assessment. Int. J. Remote. Sens. 20, 2423–2441.
Stocking, M.A., Murnaghan, N., 2001. Handbook for the Field Assessment of Land Degradation. Earthscan Publication Ltd., London (169 pp.).
Vrieling, A., 2006. Satellite remote sensing for water erosion assessment: a review. Catena 65, 2–18.
Vrieling, A., Rodrigues, S.C., Bartholomeus, H., Sterk, G., 2007. Automatic identification of erosion gullies with ASTER imagery in the Brazilian Cerrados. Int. J. Remote. Sens. 28 (12), 2723–2738.
Vrieling, A., De Jong, S.M., Sterk, G., Rodrigues, S.C., 2008. Timing of erosion and satellite data: a multi-resolution approach to soil erosion risk mapping. Int. J. Appl. Earth Obs. GeoInf. 10, 267–281.
Wischmeier, W.H., Smith, D.D., 1978. Predicting Rainfall Erosion Losses: a guide to conservationplanning. Agric. Handbook No. 282. US Department of Agriculture, Washington, DC.